Simulation of long equatorial waves in the Pacific ocean in relation with sea level oscillations and zonal mean currents

Equatorial waves
Cyclic model
Sea level variability
Altimetric data.

Ondes équatoriales
Modèle cyclique
Variabilité de la surface
Données altimétriques.

Françoise BROSSIER[a], Laurent MONIER[a] and Pascale DELECLUSE[b]

[a] LANS - Institut National des Sciences Appliquées, 20, avenue des Buttes de Coësmes, 35043 Rennes Cedex, France.

[b] LODYC - UPMC, Université Paris 6, 4, place Jussieu, 75252 Paris Cedex 05, France.

ABSTRACT

Wave-like oscillations over a period of 30 days, with a wavelength of 1 000 to 1 200 km, have been observed in the Pacific Ocean between 2°N and 4°N. Eddies with the same time-space scale are present in the sea-level oscillations observed by satellites. A numerical modelling of these long equatorial waves is presented in this paper. Fluctuations of currents and density around given mean fields are computed by a cyclic perturbation model. The oceanic response has to fit given sea-level oscillations. Three sea-level data sets have been considered : one is deduced from Geosat altimetric measurements; the other two are analytically constructed, with random time-dependence. Three mean circulations have also been studied : no mean flow, and mean circulation in the tropical Pacific during May and November.

Highly energetic eddies, on a time-space scale of 30 days-1 200 km, are obtained in November, when the meridional shear of the mean zonal current is strong. These eddies are present in the computed oceanic response whatever the sea-level data set. The 30-day period is present in the sea level observed by Geosat, but not in the theoretical sea-level data set. So, the oceanic wave is generated by the mean flow, and the sea-level anomalies, observed at the same time-space scale, are the trace of the oceanic signal. Using the mean circulation of May, or in the no-mean-flow case, the results are different. Another result given by the model concerns the heat flux associated with the perturbation. The 30 day-1 200 km eddies induce a southward heat transport principally situated north of the equator, except for a brief period. Maxima values are obtained in January-February, when the eddies are the most energetic. The eddies seem to induce a redistribution of heat in the equatorial zone which is obviously seasonally modulated, as are the eddies themselves.

RÉSUMÉ

Simulation des ondes longues équatoriales dans l'océan Pacifique. Relation avec les oscillations de surface et les courants moyens.

Des oscillations de période 30 jours, de longueur d'onde 1 000 à 1 200 km, ont été observées dans l'Océan Pacifique, entre 2°N et 4°N. Des tourbillons de même échelle sont présents dans les oscillations de la surface observées par satellites. Cet article présente une modélisation numérique de ces ondes longues équatoriales. Les fluctuations du courant et de la densité autour de valeurs moyennes données sont calculées par un modèle cyclique de perturbation. La réponse océanique doit être en accord avec des oscillations données de la surface.

Trois types de surface océanique ont été considérés : l'un est déduit des mesures altimétriques de Géosat, les deux autres sont construits de manière analytique, avec une variation en temps de type « bruit blanc ». Trois circulations moyennes ont aussi été traitées : absence de courant moyen, et circulation moyenne dans le Pacifique tropical en mai et en novembre.

Des tourbillons d'échelle 30 jours-1 200 km sont obtenus en novembre, quand le courant moyen présente un fort cisaillement méridien. Ces tourbillons sont très énergétiques, et sont présents dans la réponse océanique pour les trois types de variations de la surface que l'on a traités. La période 30 jours est présente dans les oscillations de surface observées par Géosat, mais pas dans les surfaces construites analytiquement. L'onde océanique est donc générée par le courant moyen, et les tourbillons observés en surface, à la même échelle spatio-temporelle, sont la signature du signal océanique. Les résultats obtenus pour le mois de mai, ou quand le courant moyen s'annule, sont très différents. Le modèle permet aussi de calculer le flux de chaleur associé à la perturbation. Les tourbillons 30 jours-1 200 km provoquent un transport de chaleur vers le Sud, qui, excepté durant une courte période, est localisé au Nord de l'équateur. Les flux de chaleur maximaux sont obtenus en janvier-février, quand l'activité des tourbillons est maximale. Les tourbillons semblent donc provoquer une redistribution de chaleur dans la zone équatoriale qui est, comme l'activité des tourbillons, soumise à des variations saisonnières.

INTRODUCTION

Wave-like oscillations in the current and temperature fields appear in the equatorial Pacific, Atlantic and Indian Oceans. In the eastern part of the tropical Pacific, different types of observations have shown evidence of waves with a period of about 30 days, with a wavelength of 1 000 to 1 200 km, located between 2°N and 8°N and propagating westward. Such oscillations are described in the following papers : Harvey and Patzert, 1976; Legeckis, 1977; Wyrtki, 1978; Legeckis et al., 1983; Hansen and Paul, 1984; Miller et al., 1985. More recently, such long equatorial waves have been evidenced from dynamic topography maps inferred from altimetric data (Malardé et al., 1987; Musman, 1989; Périgaud, 1990). At the same time, theoretical studies were carried out to analyse the process of equatorial instabilities. Different simulations were presented by Philander (1976, 1978), Cox (1980), Miller et al. (1985), Siegal (1985), Philander et al. (1986). All these authors obtained unstable waves in the energy-band 1 000-1 200 km, 20-30 days, and concluded that the initial eddy energy was drawn from the mean flow via horizontal shear instability between the westward SEC and the eastward NECC. The heat budget in the tropical oceans obviously depends on the heat flux associated with the eddies. Estimates of this heat flux were calculated from numerical simulations (Philander et al., 1986; Philander and Pacanowski, 1986; Philander et al., 1987). Instability waves of period 30 days, wavelength 1 000 km, were found to be effective only in the upper layer, and highly energetic for a brief period of approximately two months. A southward heat flux, in the order of 1.10^{14} Watts, was found to be induced by the eddies. However, given the small depth and the short period over which the eddies are effective, their contribution to the annual mean heat flux is small. More recently, diagrams of the eddy heat flux, deduced from the measurements of moorings located in the equatorial Atlantic, have been presented in (Dvoryaninov and Eremeev, 1992). From their pictures, we estimated, along 1°N, a southward heat transport of the order of $0.2.10^{14}$ Watts. (Note that this value is obtained by integration over one wavelength, i.e. 1 000 km, while the previous estimate, of 1.10^{14} Watts, concerns the whole ocean.)

The numerical model described in this paper permits us to compute the variability of the Tropical current system and then to obtain tropical instability. Our purpose is to study the relationship between oceanic eddies and fluctuations of the sea-level on the one hand, and oceanic eddies and mean tropical circulation on the other hand. The model is a perturbation one, which computes fluctuations of currents and density around given mean fields. The computed perturbations are not directly forced by the wind-stress, but have to correspond to given sea-level fluctuations. The external source of perturbation is then imposed in an indirect way. The equations satisfied by the perturbation are of Navier-Stokes type for velocity, and of transport-diffusion type for density. The mathematical properties of this problem (existence, unicity and regularity of the solution) have been studied by Brossier (1986 and 1987). Our purpose is to display and analyse zonal propagating waves. So, we have imposed a wave-like zonal structure for the perturbation. The resulting primitive equations model is time-dependent, bidimensional in space (latitude and depth) and cyclic in the zonal direction. Three different sea-level fluctuations have been considered. One is deduced from Geosat altimetric measurements. The other two are analytically constructed, with a random time-dependence. Three mean circulations have also been considered. The case of no mean flow permits testing of the model. The current system in the tropical Pacific is seasonally modulated: the zonal shear between the westward SEC and the eastward NECC is at a minimum in spring, and at

a maximum in autumn-winter. Perturbations of the mean flow have been computed for two typical months : May and November.

DESCRIPTION OF THE MODEL

We consider an oceanic domain extending from 9°S to 9°N, having a constant depth $H = 4000$ m. Our purpose is to use a cyclic model ; so the longitudinal extension of the domain does not matter. We assume that, at the initial time $t = 0$, there is in this tropical belt a given mean flow (U_0, ρ_0) corresponding to a mean sea-level ξ_0 . The mean current is supposed to be zonal, and averaged with respect to longitude. Velocity, density and surface topography are then given by :

$$u(x,y,z;t) = U_0(y,z) + u'(x,y,z;t) \qquad (1a)$$

$$v(x,y,z;t) = v'(x,y,z;t) \qquad (1b)$$

$$w(x,y,z;t) = w'(x,y,z;t) \qquad (1c)$$

$$\rho(x,y,z;t) = \rho_0(y,z) + \rho'(x,y,z;t) \qquad (1d)$$

$$\xi(x,y;t) = \xi_0(y) + \xi'(x,y;t) \qquad (1e)$$

(x is towards the east and y towards the north; z is vertically upward).

The equations of motion are the Navier-Stokes equations modified by the Boussinesq approximation and the hydrostatic assumption. Density has to satisfy a transport-diffusion equation. After linearization about the mean solution, the equations satisfied by the perturbation can be written :

$$u'_t + U_0 u'_x + (U_0)_y \, v' + (U_0)_z \, w'$$
$$- f \, v' - \upsilon_h \, \Delta u' - (\upsilon_v \, u'_z)_z$$
$$= - (1/\rho_m) \, p'_x \qquad (2a)$$

$$v'_t + U_0 v'_x + f \, u' - \upsilon_h \, \Delta v' - (\upsilon_v \, v'_z)_z = - (1/\rho_m) \, p'_y \qquad (2b)$$

$$u'_x + v'_y + w'_z = 0 \qquad (3)$$

$$\rho' g + p'_z = 0 \qquad (4)$$

$$\rho'_t + U_0 \rho'_x + (\rho_0)_y \, v' + (\rho_0)_z w' - \upsilon'_h \Delta \rho' - (\upsilon'_v \rho'_z)_z = 0 \qquad (5)$$

$f = 2\omega \sin \varphi$ is the Coriolis parameter, ρ_m is a mean value of the density over all the domain, $\Delta u = u_{xx} + u_{yy}$. υ_h and υ'_h are the coefficients of horizontal eddy viscosity and diffusivity. They are supposed to be constant. ($\upsilon_h = \upsilon'_h = 2.10^7$ cm^2.s^{-1}). υ_v and υ'_v are the coefficients of vertical eddy viscosity and diffusivity which are supposed to vary with respect to y and z, depending upon the vertical gradient of U_0 and ρ_0. We have used the formulation given by Pacanowski and Philander (1981) :

$$\upsilon_v = \upsilon_0 / (1+5R_i)^2 + \upsilon_B, \qquad \upsilon'_v = \tilde{\upsilon}_v / (1+5R_i) + \upsilon'_B$$

where $\upsilon_0 = 100$, $\upsilon_B = 1.84.10^{-2}$, $\upsilon'_B = 1.84.10^{-3}$, in cm^2. s^{-1}. Values of υ_B and υ'_B correspond to molecular viscosity and diffusivity. $\tilde{\upsilon}_v$ is the meridional mean of υ_v. $R_i = g((\rho_0)_z / (U_0)_z^2)$ is the Richardson number. This formulation induces more vertical mixing in the area characterized by a strong vertical shear.

If we neglect the variations of the atmospheric pressure at the sea surface, integration of equation (4) with respect to z gives us the following relation :

$$(1/\rho_m) \, \nabla p' = g \, \nabla \xi' + (1/\rho_m) \, \nabla p_h \qquad (6)$$

where $p_h = g \int_{-z}^{0} \rho' \, dz$ is the hydrostatic pressure. Relation (6) is then substituted for the expression of pressure gra-

dient in equations (2). This allows us to introduce the sea level variability $\xi'(x,y;t)$. The computed perturbations of the mean flow have to correspond to the sea level. Most oceanic PE models solve this problem either by computing an evolution equation for the sea level (Dukowicz and Smith, 1994) or by computing a new equation for the barotropic stream function, using the rigid assumption (Bryan, 1969). Both these approaches require knowledge of the wind-stress variability.

We shall take a different approach for this perturbation problem, based on the assumption of perfect knowledge of the surface pressure from the observations and computation of the oceanic flow perturbations consistent with this surface pressure forcing. Computing the response of the ocean to wind-stress forcing is not the same as computing the ocean response to a sea-level pressure anomaly. Here, we will solve the second of these problems (see appendix) and demonstrate that although not equivalent to the first problem, it is well posed, with consistent solutions between pressure fields and circulation, at least to the level of linearization considered in the present study.

Our purpose is to exhibit zonally-propagating waves. Therefore, we construct a cyclic model. Sea-level variations $\xi'(x,y;t)$ are projected on to significative zonal modes. Oceanic response, corresponding to the sea surface oscillations $\exp(imx) \, \tilde{\xi}(y;t)$, is supposed to have the same zonal variations. So, for the functions u', v',w', p' and ρ' we have the following x-dependence :

$$f'(x,y,z;t) = \exp(imx) \, |\tilde{f}| \, (y,z;t).$$

The zonal wave number, m, is fixed for each numerical run. Significant wavelengths are selected by spectral analysis of the sea-level oscillations ξ' (x,y;t) . For each of these wavelengths, we have to perform a run of the cyclic model. The periodic method reduces the initial three-dimensional problem to a two-dimensional one. For each fixed value of the wave number m, we have to solve the following equations :

$$\tilde{u}_t + im \, U_0\tilde{u} + (U_0)_y \, \tilde{v} + (U_0)_z \, \tilde{w}$$
$$- f \, \tilde{v} - \upsilon_h \, (-m^2\tilde{u} + \tilde{u}_{yy}) - (\upsilon_v \tilde{u}_z)_z$$
$$= - g \, im \, |\tilde{\xi}| - (g/\rho_m) \, im \int_{-z}^{0} \tilde{\rho} \, dz \qquad (7a)$$

$$\tilde{v}_t + im \, U_0\tilde{v} + f \, \tilde{u} - \upsilon_h(-m^2 \, \tilde{v} + \tilde{v}_{yy}) - (\upsilon_v \, \tilde{v}_z)_z$$
$$= - g \, |\tilde{\xi}|_y - (g/\rho_m) \int_{-z}^{0} \tilde{\rho}_y \, dz \qquad (7b)$$

$$im \, \tilde{u} + \tilde{v}_y + \tilde{w}_z = 0 \qquad (8)$$

$$\tilde{\rho}_t + im U_0\tilde{\rho} + (\rho_0)_y \, \tilde{v} + (\rho_0)_z \, \tilde{w} - \upsilon'h(-m^2 \, \tilde{\rho} + \tilde{\rho}_{yy})$$
$$- (\upsilon'v \, \tilde{\rho}_z)_z = 0 \qquad (9)$$

Computations are made using complex variables. The physically significant perturbation corresponding to each complex function $\tilde{f}$ (y,z;t) = f_1 + if_2 is given by : f' = f_1 cos mx $- f_2$ sin mx.

Numerical space discretization is performed using a finite difference formulation and a staggered network. The meridional step Δy is constant and equal to 0.5° of latitude. In the vertical, we use variable space steps in order to obtain more grid points in the mixed layer and at the level of the thermocline, where variations are very important, and less grid points below. Density and horizontal velocity are computed at the following depths : 5, 15, 25, 36.25, 51.25, 70, 90, 110, 130, 150, 172.5, 217.5, 325, 550, 950, 1500, 2150, 2850, 3550 m (19 levels). Vertical velocity is computed at intermediate levels.

At the northern and southern boundaries located at 9°N and 9°S, slip conditions are applied :

$$u'_y = 0 \ ; \quad \rho'_y = 0 \ ; \quad v' = 0 \ \text{at } 9°N \text{ and } 9°S \tag{10}$$

At the depths z = 0 and z = 4 000 m, we assume that the perturbation has no vertical gradient : $u'_z = v'_z = \rho'_z = 0$ (11)

In order to get w', by integrating equation (8) with respect to z, we assume : w' = 0 at z = 4000 m. (12)

A justification of these vertical boundary conditions is given in the appendix. It has to be noted that no conditions are specified on the free surface $z = \xi_0 + \xi'$.

At initial time t = 0, the disturbances are zero. So, the initial conditions are given by :

$$u' = v' = w' = \rho' = 0 \quad \text{at } t = 0 \tag{13}$$

For time discretisation, we use the implicit Crank-Nicolson scheme. All numerical experiments have been carried out with a time step $\Delta t = 900$ s.

NB: *Notation " ' " used for the perturbation of the mean situation will now be omitted.*

MEAN CIRCULATION

Three different mean flows are considered in order to display the relation between the excited waves and the characteristics of the mean flow.

No mean current

$U_0(y,z) = 0$. The density profile $\rho_0(z)$ is given as typical of the tropical Pacific Ocean with a sharp pycnocline at a depth of about 100 m.

Mean current : tropical Pacific in May

Current $U_0(y,z)$ and density $\rho_0(y,z)$, are given by the three-dimensional model of the Pacific Ocean developed in LODYC (Laboratoire d'Océanographie Dynamique et Climatologie, Université Paris 6) and described by Dandin (1991). The mean zonal current U_0 is plotted on Figure 1a. The equatorial undercurrent is centred on the equator. Its maximum speed is located at a depth of 80 m and exceeds
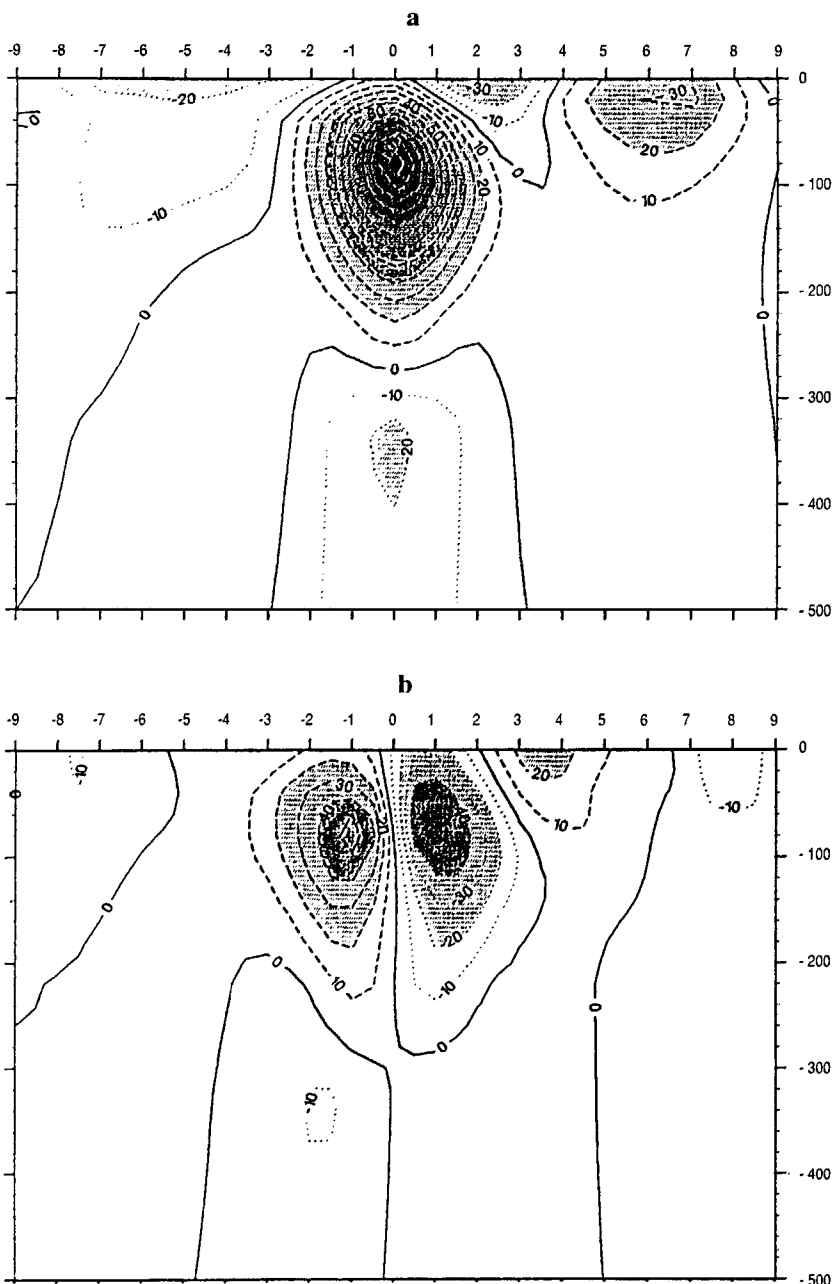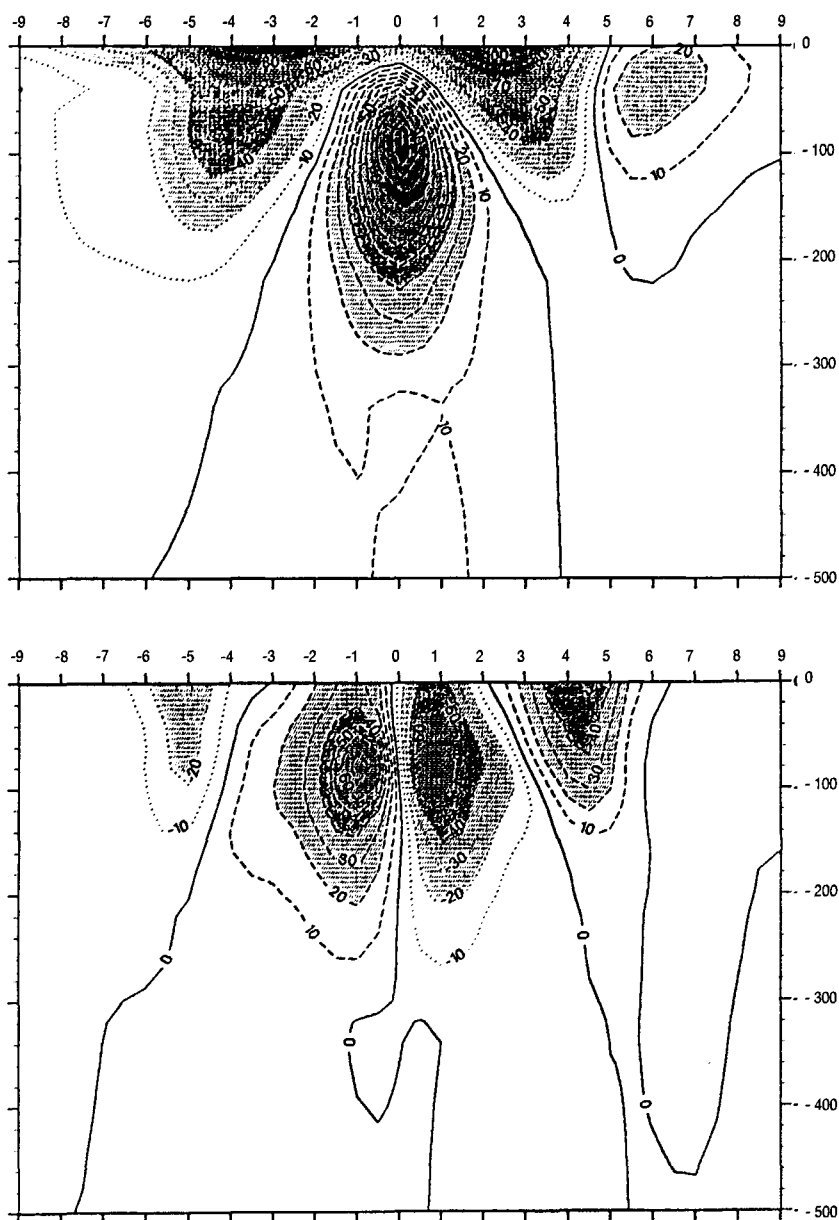

Figure 1

Mean flow in the tropical Pacific in May, as a function of latitude (9°S-9°N) and depth (0-500m):
a - Zonal velocity U_0;
dotted lines : U_0 westward ; dashed lines: U_0 eastward ; contour interval is $10 \ cm.s^{-1}$.
b - Meridional shear $(U_0)y$; contour interval is $10.10^{-7} \ s^{-1}$.

Figure 2

Mean flow in the Tropical Pacific in November; similar to Fig. 1.

100 cm/sec. The undercurrent extends up to the surface. Westward currents are weak. Maximum speeds of about 20 to 30 cm.s^{-1} are observed between 7°S and 3°S and between 1°N and 3°N. The vertical extension of these westward currents is weak. The NECC can be seen between 4°N and 8°N. It extends down to a depth of 100 to 200 m. Its maximum speed is about 30 cm.s^{-1} The meridional shear $(U_0)y$ is plotted on Figure 1b. Maxima values of about 5.10^{-6}. s^{-1} are observed at 1°S and 1°N. They are connected with the undercurrent. The gradient associated with the NECC is not very important : its maximum, equal to 2.10^{-6} s^{-1}, is located near the surface between 3°N and 4°N ; these values decrease quickly with depth.

Mean current : tropical Pacific in November

The zonal current U_0 and its meridional shear $(U_0)y$ are plotted on Figure 2. The equatorial undercurrent is deeper than in May, its core being located at 90 m. The values of the eastward velocity are nearly the same as in May. There is a strong vertical shear on the equator : the surface current is westward, opposite the eastward undercurrent.

Westward currents are much stronger than in May : velocities of about 100 cm.s^{-1} are observed in the surface layer between 4°S and 2°S and between 1°N and 3°N. The vertical extension of these westward currents is also greater than in spring. The NECC appears between the latitudes of 5°N-9°N and the depths of 0-200 m. It is nearly the same as in May. The intensification of westward currents induces an increase of the meridional shear $(U_0)y$. The maximum associated with the NECC is much stronger than in May, with values of about 4.10^{-6} s^{-1} between 3°N and 5°N, and a vertical extension of 150 m.

SEA-LEVEL VARIABILITY

The numerical model calculates the perturbation of the mean velocity and density fields, corresponding to fluctuations of the sea surface given by : $\xi(x,y;t) = \exp(imx)$ $|\xi|(y;t)$. All the results described from now on have been obtained for a wavelength $\lambda = 1\,200$ km (m = 5.2 . 10^{-8} cm^{-1}). This choice will be justified later.

Three sea-level variabilities have been considered. The first two are theoretical: antisymmetrical (sea level 1) and symmetrical (sea level 2) about the equator, with a random time dependence. The meridional profile of ξ is given as a regular function of latitude, vanishing at 9°S, 0° and 9°N, and with a maximum outside the equatorial wave guide. Corresponding fluctuations ξ (y;t) are plotted on Figure 3. The assumption of antisymmetrical or symmetrical sea-level oscillations makes it possible to excite separately even and odd meridional modes. These numerical experiments extend over 301 days in order to perform Fourier transforms of the perturbation and to exhibit low-frequency waves.

Eventually, the case of sea-level oscillations deduced from Geosat data (sea-level 3) has been considered. Geosat data were corrected and filtered at the Jet Propulsion Laboratory, (Périgaud, 1990). From this Geosat analysis, maps of the sea-level oscillations in the tropical Pacific (15°S-15°N) were obtained with a time-space resolution of 10 days and 1°, from October 1986 to January 1989. In order to analyse waves present in the sea-level variability and to separate the main modes, we performed a Fourier analysis of the altimetric signal, with respect to time and longitude. The sea-level variability $\xi(x,y;t)$ is then filtered in different energy bands. Only wavelengths and periods lower than 2000 km and 100 days have been considered. Two energy highs are identified in the eastern basin : one along 5°N for periods of 30-40 days and wavelengths of 1 000-2 000 km (band 1), the latter along 12°N for periods of 50-80 days and wavelengths of 700-1 000 km (band 2). From now on, we will be dealing with energy band 1 only. The energy level is much lower in the western basin where no significant energy peak is present. Figure 4 presents the signal filtered in energy band 1, along 5°N. Waves vanished during

the spring of 1987 (1987 is known to be a El Niño year, and consequently the meridional current shear is expected to be low and the waves activity to be reduced). Waves were the most active from September 1987 to February 1988 and weakened during the spring of 1988. In order to obtain the most significant signal, the period September 1987 to February 1988 was selected. The orientation of phase lines shows a westward phase speed of 35 km/day. An eastward group velocity of 30 km/day is determined from the displacement of maxima values (Périgaud, 1990). This bidimensional Fourier analysis allows us to select a dominant wavelength (we chose $\lambda = 1\,200$ km which corresponds to the most significant signal) and to determine the area and time period in which waves are the most active : the eastern basin of the tropical Pacific from October 1987 to February 1988. The sea-level variability imposed in the cyclic model is obtained by projecting the Geosat signal on to the wavelength 1 200 km. The resulting filtered oscillations are plotted on Figure 5. The signal is weak south of the equator and in the equatorial band. A wave with a period of about 32 days can be seen in the zonal band 3°N-8°N. Its maximum is located along 5°N-6°N.

RESULTS

Perturbations of velocity and density have been calculated for the three mean fields (U_0, ρ_0) and the three sea-level variabilities previously described. Computations have been performed over a period of 301 days for theoretical sea-levels 1 and 2, 141 days for the Geosat sea-level 3.
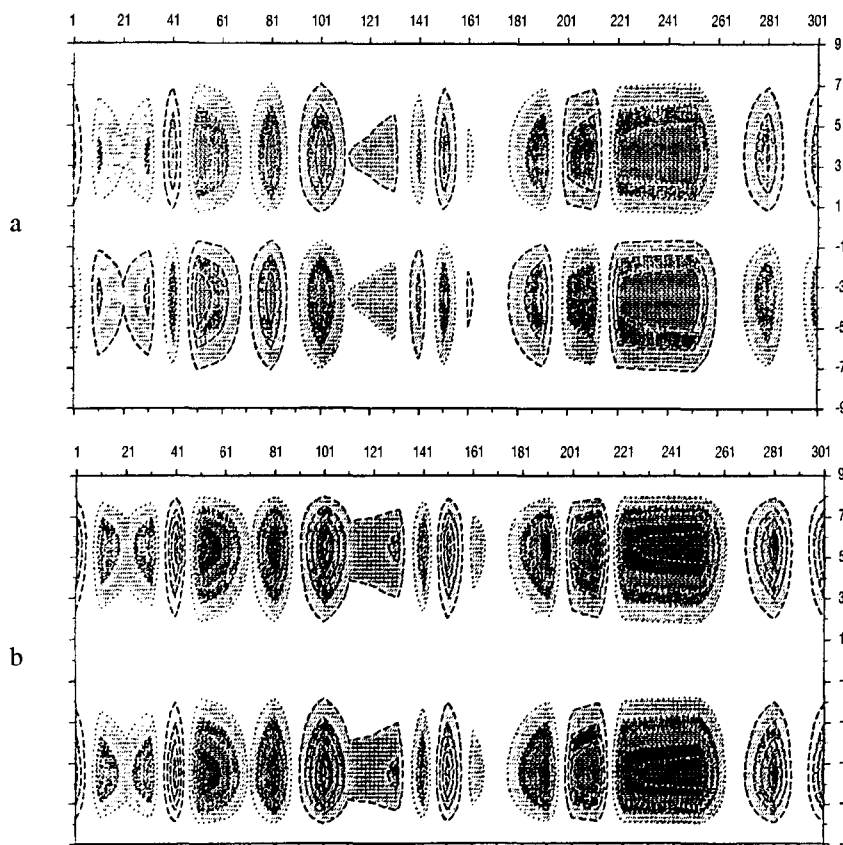

Figure 3

Sea-level oscillations ξ as a function of latitude (9°S-9°N) and time (301 days), at a fixed longitude (x=0).
Dotted lines : $\xi < 0$; dashed lines: $\xi > 0$; the zero line is not plotted ; contour interval is 0.5 cm.
a - sea-level variability 1 ; b - sea-level variability 2.

No mean current

In order to display oceanic waves, for the three different sea levels, we plotted the kinetic energy of perturbation corresponding to the meridional component, and integrated over one wavelength (Fig. 6) :

$E_v = (\rho_m/2\lambda) (\int v^2 dx)$. The results are quite different, depending on the sea-level : on Figure 6a, we observe a concentration of energy, with maxima greater than 200 g.s^{-2} in the equatorial band 1°S-1°N. The energy plotted on Figure 6b is much weaker and the location of its maxima, at 5°S and 5°N, corresponds to the maxima of the sea-level fluctuations. Figure 6c shows a maximum of energy in the band 2°S-3°N, with maxima values of 100 to 200 g.s^{-2}. Outside this area, the kinetic energy remains weak.

Figure 7 presents the poleward heat transport induced by the perturbation : $H = \rho_m C_p \int\int v \theta dx dz$, integrated over one wavelength and over the depth 4000 m (temperature θ is deduced from density ρ using a state equation). We observe on Figure 7a (sea-level 1) an antisymmetrical heat transport, converging towards the equator. Maxima values of 20 to 30.10^{12} Watts are located in the equatorial band, corresponding to the maximum of kinetic energy E_v observed on Figure 6a. The heat transport plotted on Figure 7b (sea-level 2) is also converging towards the equator, but it is much weaker : maxima of 5.10^{12} Watts located at 5°S and 5°N and corresponding to the maxima of energy E_v. For sea-level 3 (Fig. 7c), the equatorial band remains a zone of convergence. Some exchanges between the northern and southern hemispheres can be observed in the areas where kinetic energy is strong.

The analytical theory of equatorial modes is valid in the case of no mean current (Lighthill, 1969). So, we can analyse the behaviour of the v component of the velocity within the theory. Time dependence of v corresponds in part to the sea-level fluctuations $\xi(t)$, but free equatorial modes are also present.

In the case of sea level 1, v is symmetrical about the equator and only even meridional modes are present. Performing a Fourier analysis of the time series v(t), we obtain three energy peaks corresponding to two westward-propagating waves of periods 43 and 33 days and one eastward-propagating wave of period 27 days. These waves are centred on the equator and correspond to the maximum of kinetic energy E_v , observed in the equatorial band 1°S-1°N. Figure 8 presents the vertical structure of v along the
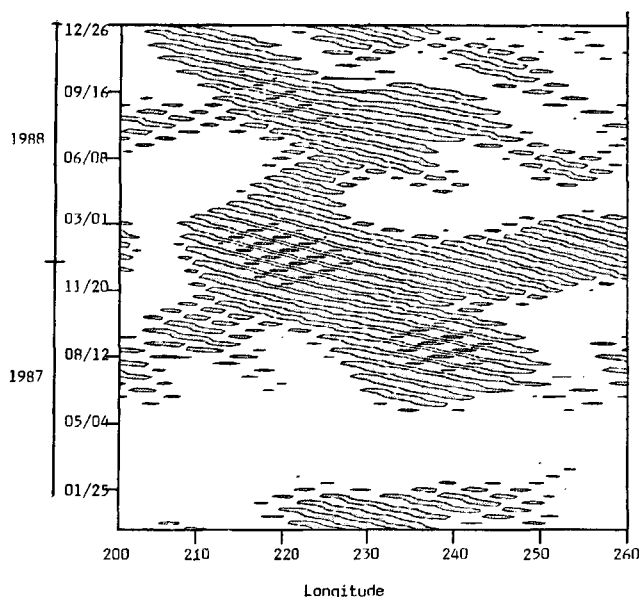

Figure 4

Geosat data: sea-level variations, filtered in the band 1000-2000 km, 30-40 days, as a function of longitude and time, at a fixed latitude (5°N). Isocontours are: -5, -3, -1, 1, 3, 5 cm.

equator. A vertical propagation can be observed, which we shall now compare with the analytical theory of equatorial modes. According to this theory, the current velocity can be represented as an expansion of meridional modes that are either vertically trapped or vertically propagating. Following Cox (1980), the Yanaï wave 1 200 km - 30 days is characterized by an equivalent depth h = 3.36 cm, a westward phase velocity equal to 40 km/day, an eastward group velocity equal to 15.4 km/day. Its vertical wavenumber k depends upon vertical stratification. It reaches a minimum value k = 200 m at the level of the pycnocline, about 100 m. Then, k increases with depth and we get k = 500 m at a depth of about 1 000 m. The vertical phase velocity is upward. Its value decreases from 10 m/day to 7 m/day, between the sea surface and z = 100 m. Then it increases and is approximately equal to 17 m/day at depth z = 1 000 m. The vertical group velocity is downward. Its value is weak : 2 m/day at z = 100 m, 5m/day at z = 800 m. The study of the vertical structure of v on the equator gives orders of magnitude similar to the theoretical values.
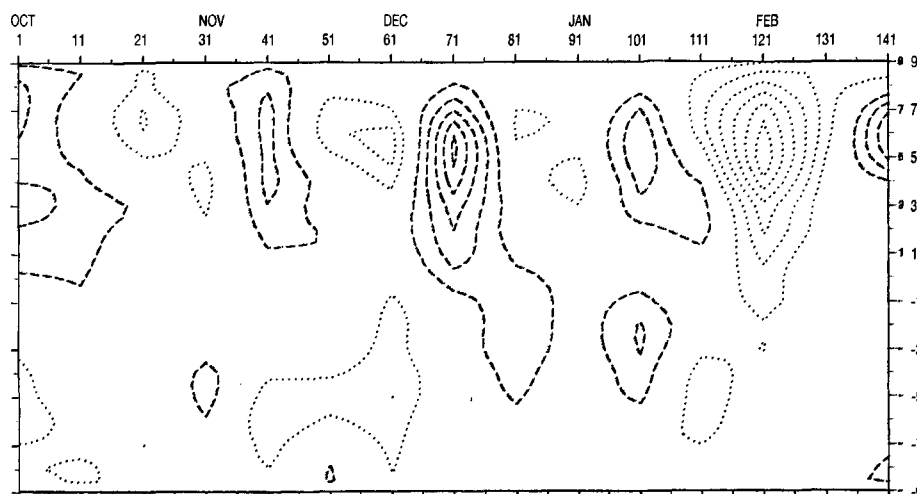

Figure 5

Sea-level variability 3: sea-level oscillations ξ as a function of latitude (9°S-9°N) and time (1 October 1987 to 18 February 1988), at a fixed longitude (x=0).

Dashed lines: ξ < 0 ; dotted lines: ξ > 0 ; the zero line is not plotted ; contour interval is 1 cm.

467

However, the results of the numerical model cannot correspond totally to the analytical theory, since we are unable to isolate one particular mode without projecting the surface signal on to this mode. As stated previously, energy spectra obtained by Fourier analysis of v show that several modes are superimposed.

In the case of sea level 2, v is antisymmetrical about the equator and only odd meridional modes can be present.

The time dependence of the fluctuation of the velocity depends mainly on the fluctuation of the sea-level. However, spectral analysis gives one energy peak corresponding to a period of 30 days. This wave is present along 1°30 N and along 4-5°N but its density of energy is small.

The v component obtained with sea-level 3 is presented in Figure 9. The values of v are low in the band 3°N-7°N where the sea-level fluctuations are the highest. Most of v
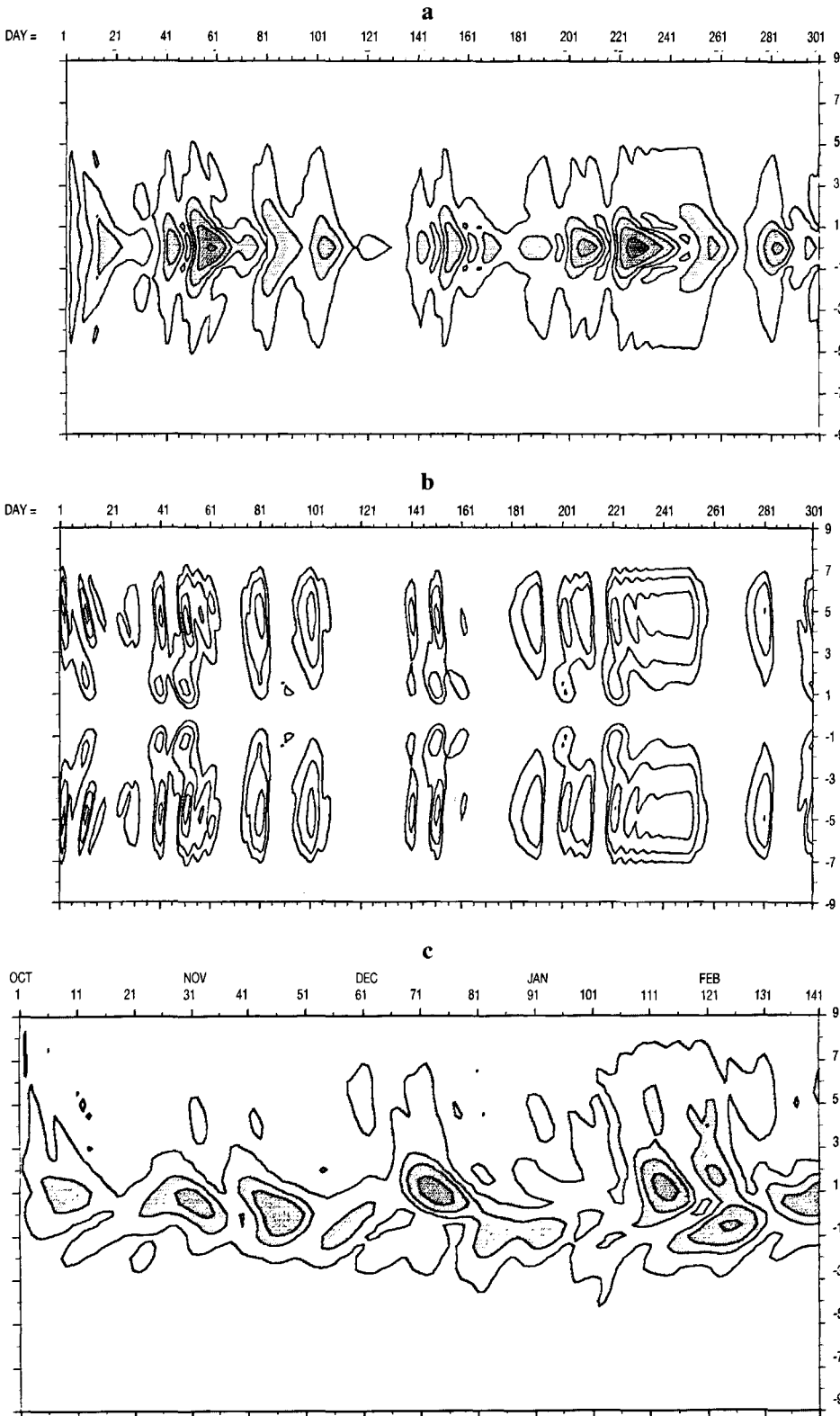

Figure 6.

$U_0 = 0$

Energy E_v as a function of latitude and time, at a fixed depth ($z=5$ m). Shaded areas : $E_v > 50$ g.s^{-2}.

a - sea-level 1 (301 days). Isocontours are 10, 50, 100, 200, 400 g.s^{-2}.
b - sea-level 2 (301 days). Isocontours are 5, 10, 20, 30, 40 g.s^{-2}.
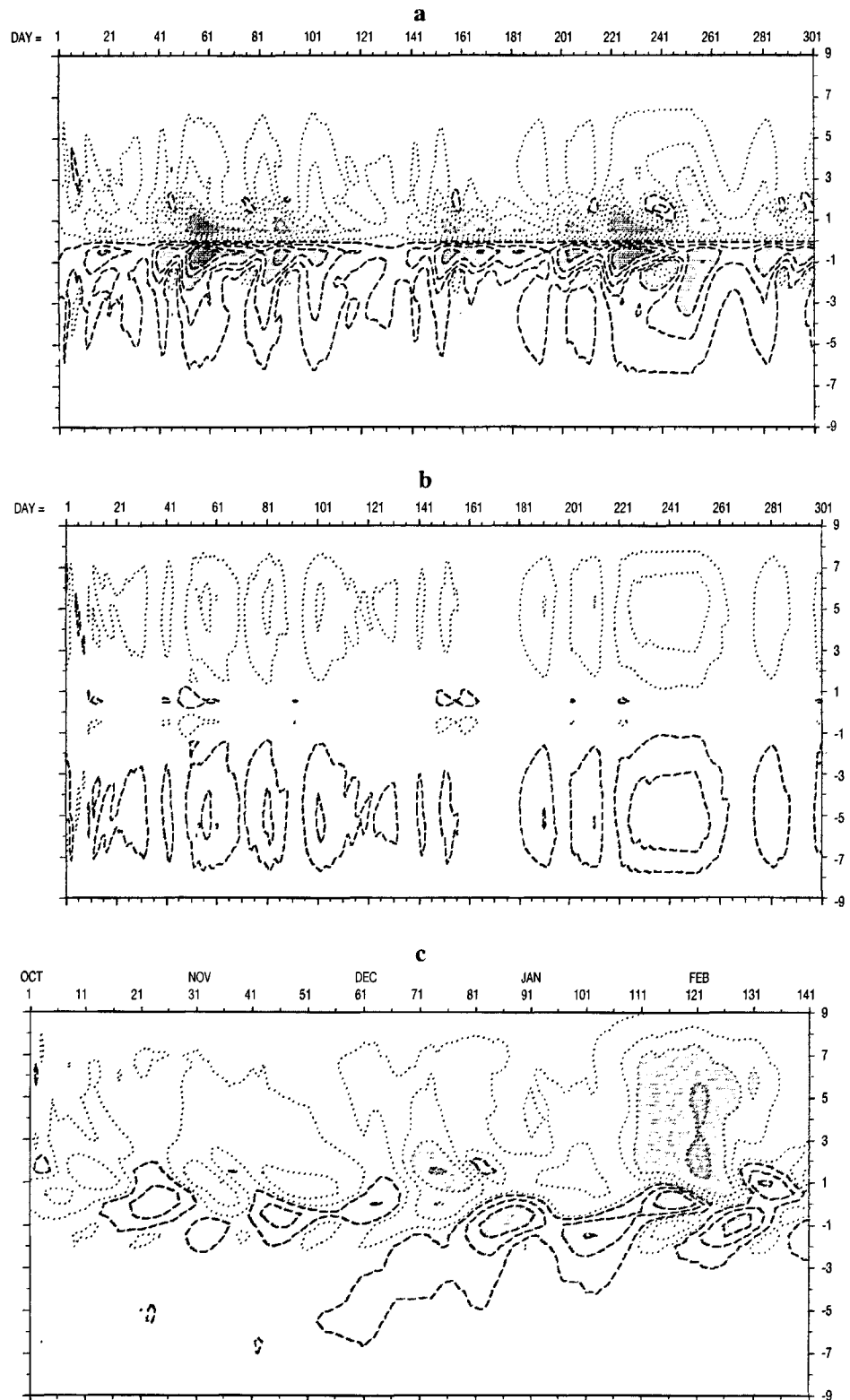*c - sea-level 3 (141 days: 1 October 1987 to 18 February 1988). Isocontours are 10, 50, 100, 200, 400 g.s^{-2}.*

Figure 7.

$U_0 = 0$

Heat transport H as a function of latitude and time.
Dotted lines: H southward ; dashed lines: H northward ; isocontours are -30, -20, -10, -5, -1, 1, 5, 10, 20, 30. 10^{12} Watts ; shaded areas : $|H| > 10.10^{12}$ Watts.

a - sea-level 1 ; b - sea-level 2 ; c - sea-level 3

dynamics is located in the equatorial band, with a succession of positive and negative values. We can observe on Figure 9b, particularly from 15 January to 18 February, a vertical propagation which corresponds to the analytical theory of equatorial modes and with the results previously described for sea-level 1. Figure 9b also shows that v decreases quickly with depth. A Fourier analysis of v has been performed in the equatorial band. Time series are shorter than for sea-levels 1 and 2 (141 days), so it is more difficult to separate the excited frequencies. The analysis

of energy spectra shows that several waves are superimposed with periods ranging from 20 to 40 days.

Mean current : Pacific in May

The kinetic energy of perturbation E_v is presented in Figure 10. Comparing Figure 10a with Figure 6a, we observe that the mean current destroys the symmetry and induces a strong weakening of the equatorial phenomena. E_v now presents two maxima : one is located in the equatorial band
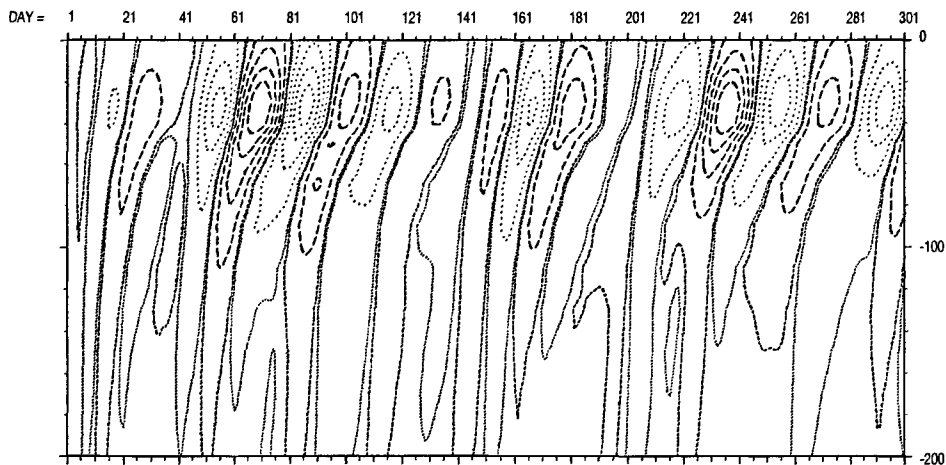
Figure 8.

$U_0 = 0$, sea-level 1.

Meridional component of velocity v along the equator and at a fixed longitude (x=0) as a function of depth (0-200 m) and time. Dotted lines: v southward ; dashed lines: v northward ; isocontours are -40, -30, -20, -10, -2, 2, 10, 20, 30, 40 cm.s^{-1}.

1°S-1°N but its energy is about four times as weak as in the case $U_0 = 0$; the other is centred on 2°N. Two energy peaks, corresponding to the 18- and 30-days periods, are present in the v spectra. The maximum of spectral density of energy is along 2°N, in the area where the kinetic energy E_v is strong. The introduction of the mean circulation induces almost the same effects for sea-level 3 : the energy E_v is much weaker in the equatorial band than in the case $U_0 = 0$. We observe on Figure 10c two maxima : one along 1°S, and another, stronger, centred on 3°N. The results

obtained with sea-level 2 (Fig. 10b) are not greatly modified by the introduction of the mean current: phenomena are weakened in the southern hemisphere and intensified in the northern hemisphere. The kinetic energy E_v is maximum between 1°N and 4°N. Maxima values, about 40 g.s^{-2}, remain much weaker than for sea-level 1. Fourier analysis of v displays two energy peaks, corresponding to periods of 18 and 30 days, with a maximum along 2°N. Periods and location of these waves are the same as for sea-level 1 but the density of spectral energy is twice as weak. Figure 11
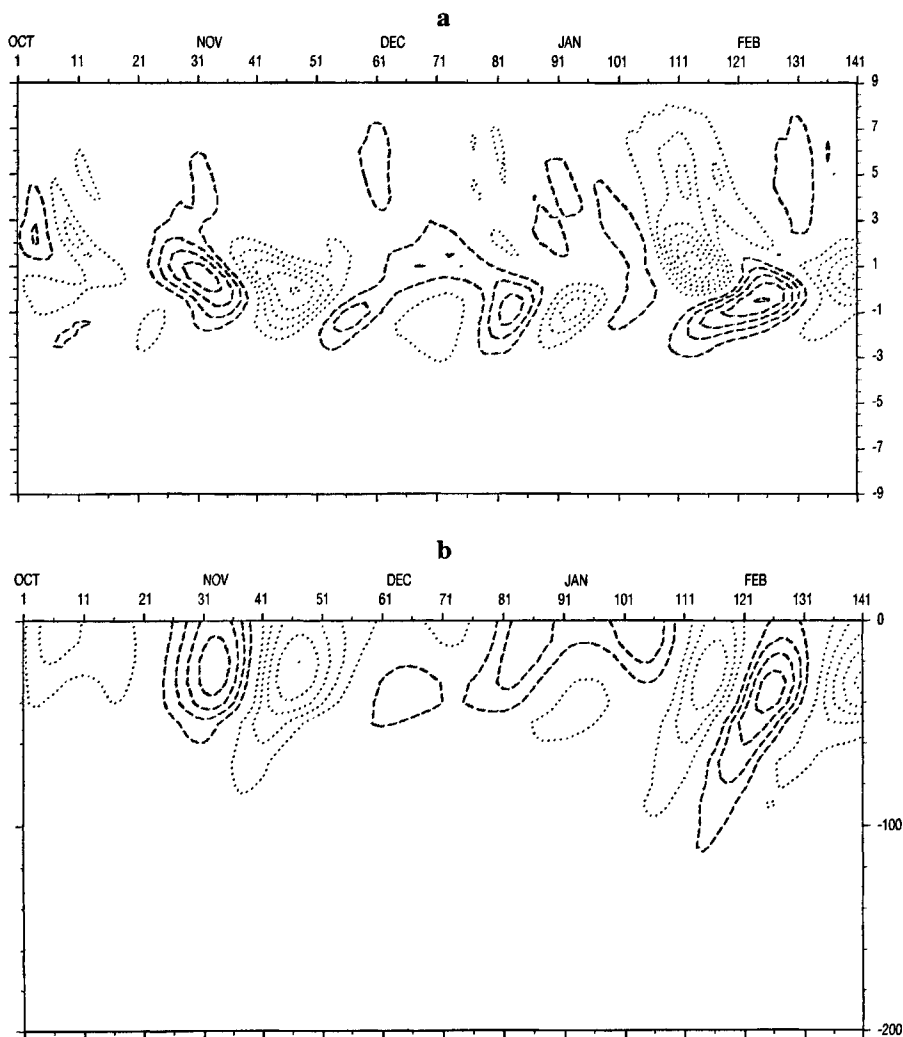

Figure 9.

$U_0 = 0$, sea-level 3.

Meridional component of velocity v at a fixed longitude (x=0). Dotted lines: v < 0 ; dashed lines: v > 0 ; the zero line is not plotted ; contour interval is 5 cm.s^{-1}.
a - v as a function of latitude and time, at a fixed depth (z = 25 m). b - v as a function of depth (0-200 m) and time, along the equator.

Figure 10.

Mean flow : May.

Energy E_v as a function of latitude and time, at a fixed depth ($z = 5$ m). Shaded areas : $E_v > 50$ g.s^{-2}.

a - sea-level 1. Isocontours are 10, 50, 100, 200, 400 g.s^{-2}. b - sea-level 2. Isocontours are 5, 10, 20, 30, 40 g.s^{-2}. c - sea-level 3. Isocontours are 10, 50, 100, 200 g.s^{-2}.
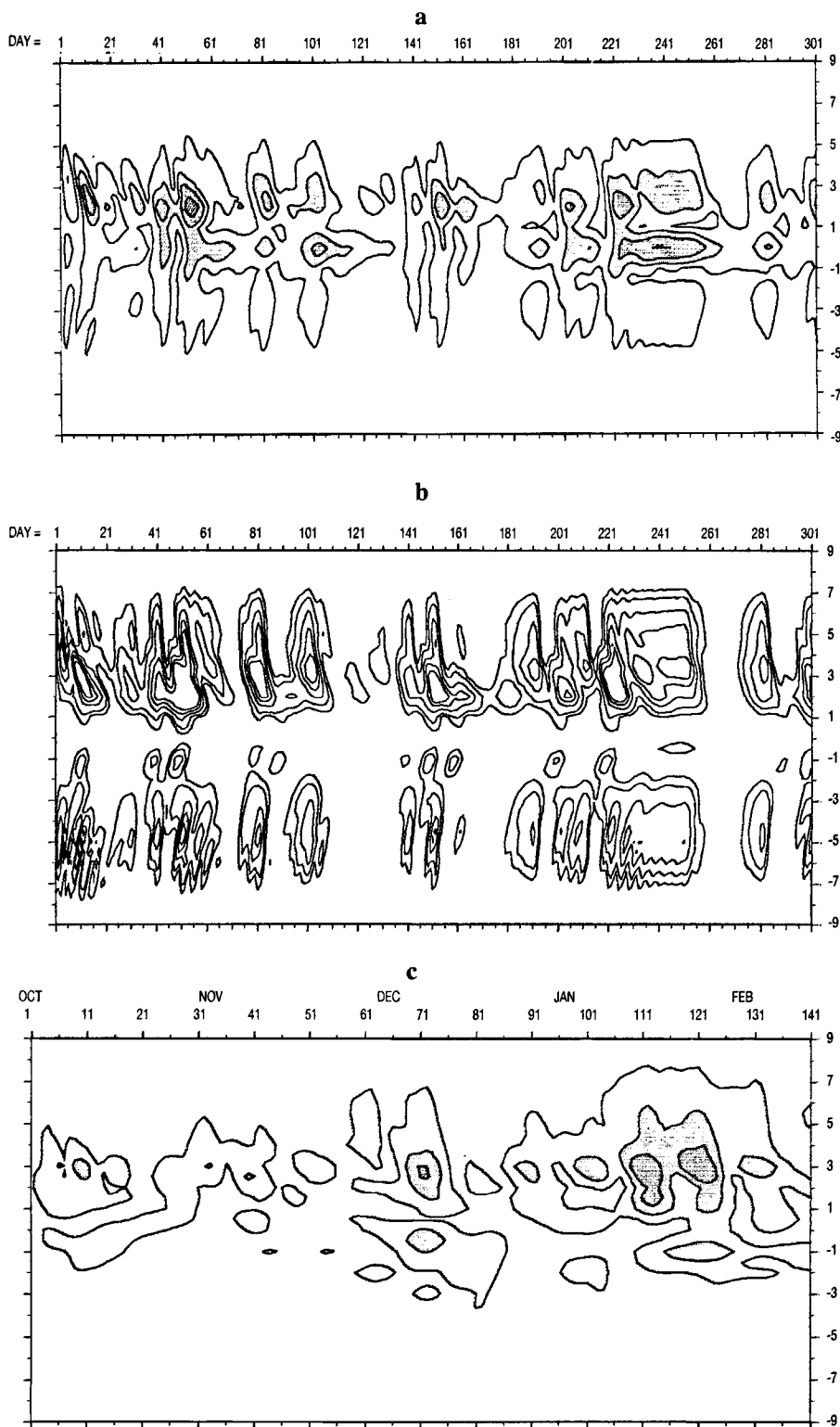
represents the heat transport H induced by the perturbation. Comments are the same as previously: the mean circulation induces a strong decrease of equatorial phenomena, with a slight increase in the area 3°N-6°N.

Mean current : Pacific in November

Figure 12 is to be compared with Figures 6 and 10. The influence of the mean current is obvious : the three maps *a*, *b* and *c*, obtained with the three sea-level variabilities 1, 2 and 3, present the same characteristics. The equatorial

concentration of energy observed on Figures 6*a* and 6*c*, still present but weak on Figures 10*a* and 10*c*, has completely disappeared on Figures 12*a* and 12*c*. E_v remains weak in the southern hemisphere. On the three maps, we observe a strong concentration of energy between 2°N and 4°N. The total energy of perturbation

$$E = (\rho_m/2\lambda) \int (u^2 + v^2 + w^2)dx - g/(2\lambda(\rho_0)_z) \int \rho^2 \, dx$$

is trapped in the upper layer (0-100 m).

We then analysed the v component of the velocity in order to determine whether the maximum of energy observed in

471

the band 2°N-4°N was associated with an oceanic wave. Fourier analysis displays, for sea-levels 1 and 2, a single energy peak corresponding to a period of about 30 days. These periodic oscillations can be seen on Figure 13, which represents the vertical structure of v, at the latitude of strongest energy. In the case of Geosat sea-level 3, time series are shorter and it is difficult to separate such periods. However, the drawing of v at depth z = 5 m (Fig. 14a) clearly shows oscillations of period 30 to 40 days along 3°N, where the maximum of energy is observed. These oscillations also appear on the vertical section (Fig. 14b). The vertical structure of v displays no vertical propagation of these oscillations and corresponds to the trapping of energy in the upper layer.

Finally, we have computed the perturbation heat transport H, integrated over one wavelength and the depth 4000 m. The heat flow is much stronger in the northern than in the southern area. For theoretical sea-levels 1 and 2 (Fig. 15a,b) a northward heat transport sometimes appears in the band 2°N-3°N, corresponding to the maxima of kinetic energy observed on Figure 12a,b. The maximum heat flux is southward and located between 3°N and 7°N. There is no interhemispheric heat exchange. In the case of Geosat sea-level (Fig. 15c), we observe a strong southward heat transport, especially in January and February. This phenomenon appears where the oscillations of period 30-40 days are most active. This southward heat flow crosses the equator.

DISCUSSION

In this paper, fluctuations of current and density fields in the tropical Pacific Ocean are calculated using a cyclic perturbation model. The variability of the sea-level is specified and the computed perturbations have to correspond to this surface signal. Depending on the characteristics of the mean tropical circulation, different waves are present in the oceanic response.

In the absence of mean flow, we obtain, for antisymmetrical and Geosat sea-level variabilities, even meridional modes, trapped on the equator. When the numerical run is long enough, (sea-level 1 : 301 days) different modes can be separated by Fourier analysis. The most energetic wave, for the fixed wavelength 1 200 km, has a period of about 30 days and is probably a Yanaï wave, as described by Cox (1980). For a shorter numerical run (Geosat sea-level 3 : 141 days), it is difficult to separate such modes of periods 20 to 40 days by spectral analysis. However such oscillations appear in the mapping of v-contours, along the equator. The maximum of the surface signal is located along 3°30 S and 3°30 N in case 1, between 5°N and 6°N in case 3. The meridional component of the velocity is weak in these areas. Kinetic energy associated with v is trapped in an equatorial band, i.e. in a zone where the sea-level signal either vanishes (sea-level 1) or is weak (sea-level 3). In the
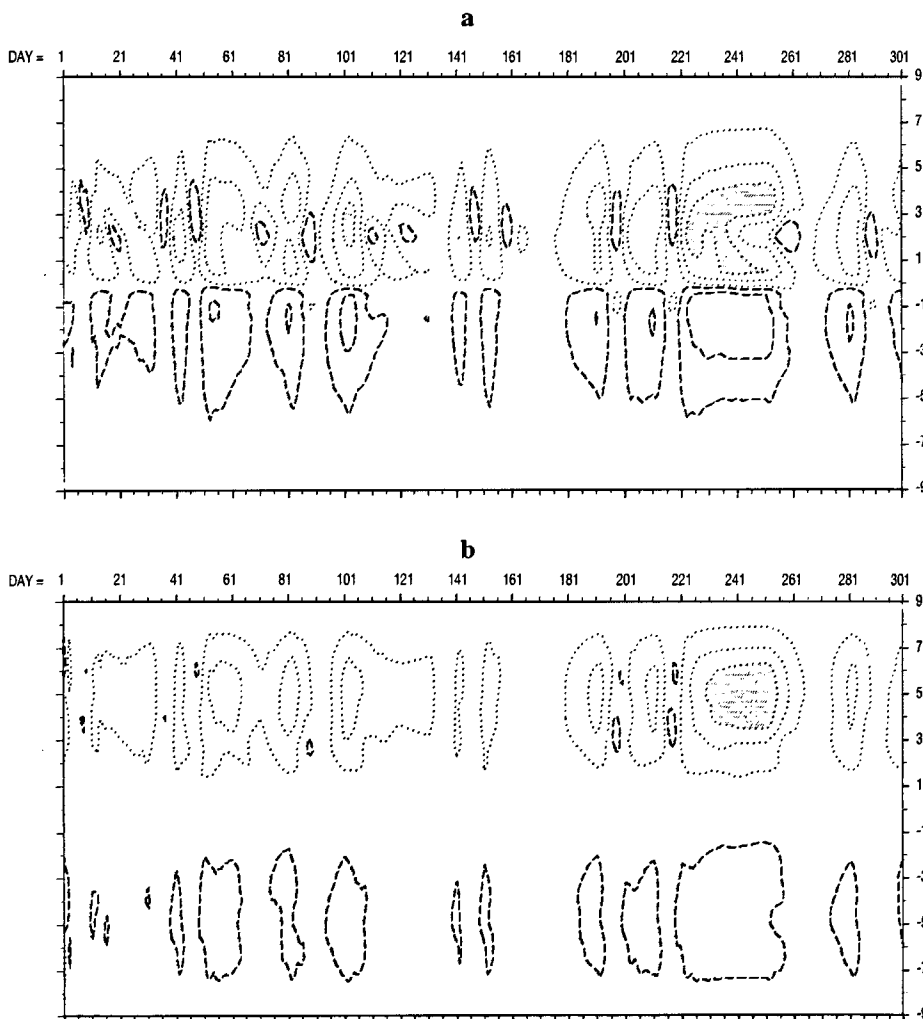

Figure 11.

Mean flow : May.

Heat transport H as a function of latitude and time. Dotted lines: H southward ; dashed lines: H northward ; isocontours are -10, -5, -1, 1, 5, 10.10^12 Watts ;
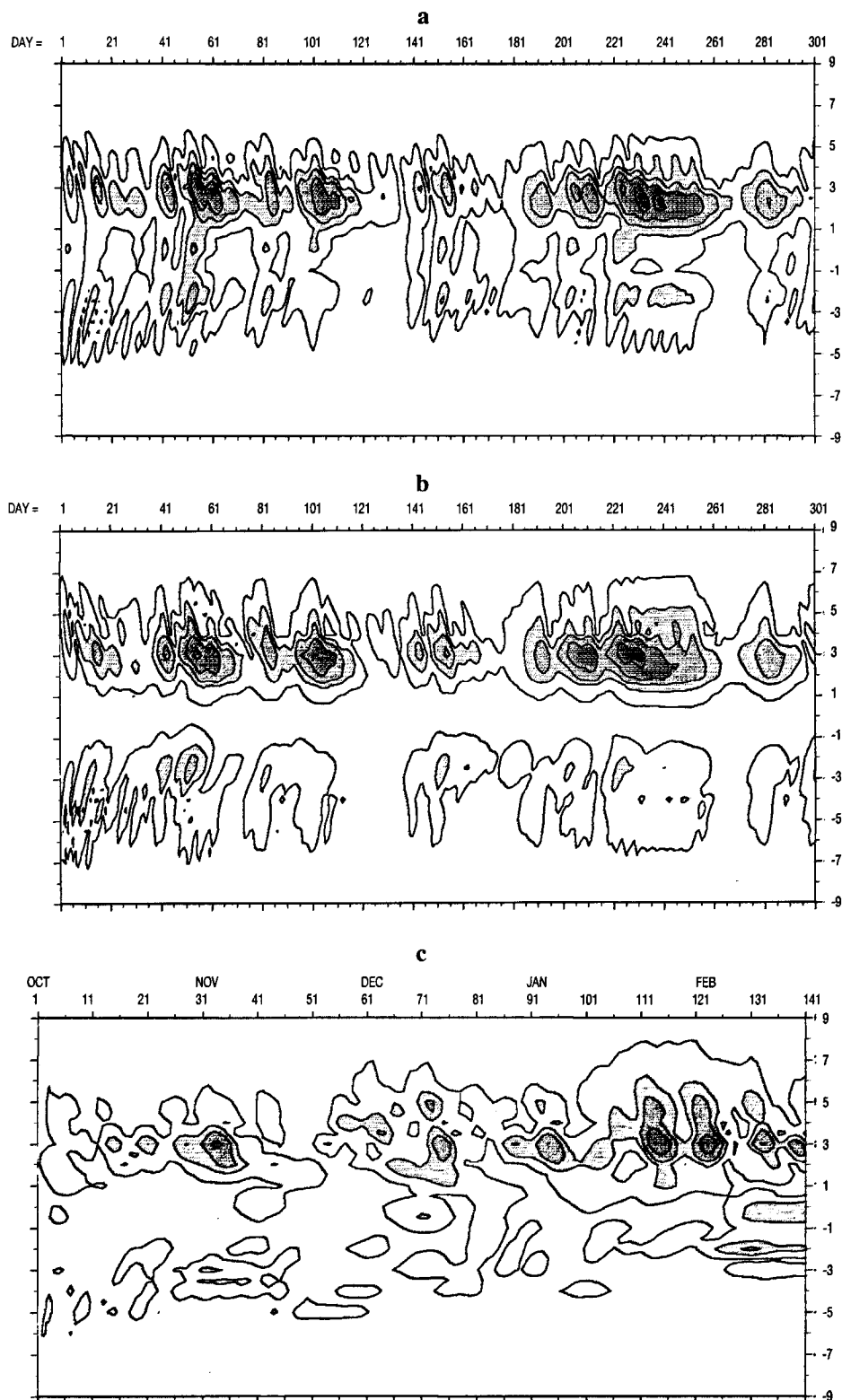
a - sea-level 1 ; b - sea-level 2.

Figure 12.

Mean flow : November.

Energy E_v as a function of latitude and time, at a fixed depth ($z = 5$ m). Isocontours are 10, 50, 100, 200, 400 $g.s^{-2}$; shaded areas: $E_v > 50$ $g.s^{-2}$.

a - sea-level 1 ; b - sea-level 2 ; c - sea-level 3.

case of symmetrical sea-level 2, time dependence of v corresponds mainly to the sea-level oscillations. Odd meridional modes are still present, but less energetic than the even modes previously described.

The introduction of the mean flow in the Tropical Pacific during May destroys the symmetry about the equator and reduces the amplitude of the equatorial signal. The even meridional modes, obtained in the absence of mean flow, are still present, but much weaker. Another phenomenon appears : for theoretical sea-levels 1 and 2, we get two

energy peaks along 2°N corresponding to the periods 18 and 30 days. The energy is rather high for sea-level 1, small for sea-level 2. For Geosat sea-level 3, the same kind of signal is observed along 3°N. The only change in the numerical model being the introduction of the mean flow, these oscillations, along 2 and 3°N, seem to be connected with the characteristics of the mean current.

The most interesting results are obtained with the mean flow of November. The equatorial phenomenon has completely disappeared : even modes, trapped along the equa-
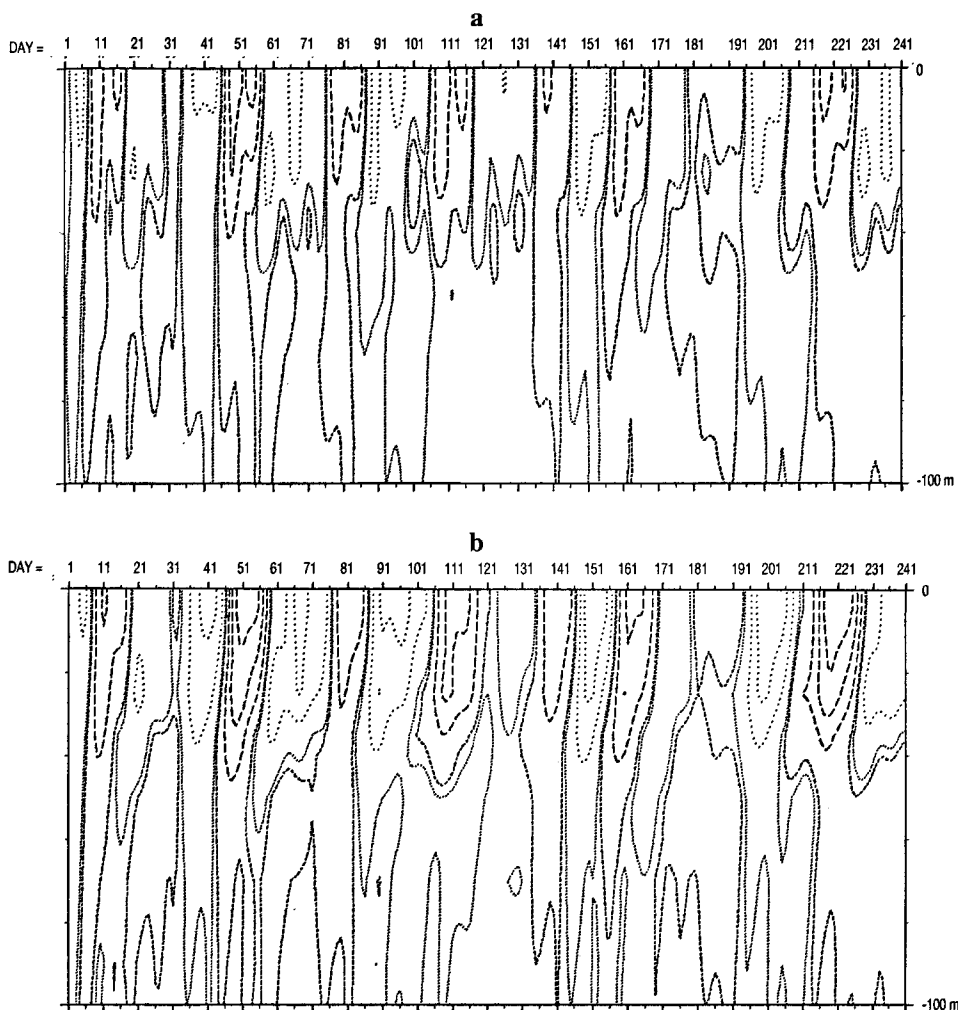
a

DAY = 1 11 21 31 41 51 61 71 81 91 101 111 121 131 141 151 161 171 181 191 201 211 221 231 241

Figure 13.

Mean flow : November.

v as a function of depth (0-100 m) and time (241 days), at a fixed latitude and longitude. Dotted lines: v < 0 ; dashed lines: v > 0 ; isocontours are -30, -20, -10, -2, 2, 10, 20, 30 cm.s⁻¹.

a - sea-level 1 ; latitude 2°30 N. b - sea-level 2 ; latitude 3°N.

b

DAY = 1 11 21 31 41 51 61 71 81 91 101 111 121 131 141 151 161 171 181 191 201 211 221 231 241

tor, are no longer present. Whatever the sea-level variability, the response of the model is characterized by a concentration of energy in the band 2°N-4°N. This energy peak corresponds to a wave of imposed wavelength 1 200 km and of period about 30 days. Such a wave 1 200 km-30 days was observed in May along 2°N but its energy was much weaker than in November. This wave appears for the 3 different sea-level variabilities that we have imposed. Thus, it has to be connected with the mean flow, which is characterized in November by an intensification of the westward currents and a strong meridional shear due to the presence of the eastward NECC alongside the westward SEC. The wave 1 200 km-30 days is located along 3°N, in the core of the westward current.

The eddies exhibited by our model mainly depend on the characteristics of the mean flow. Another approach founded on different assumptions was recently developed in (Mc Creary and Yu, 1992). They used a non-linear 2 1/2 layer model to study the dynamics of equatorial circulation, including the generation of mean flow and instabilities. The forcing of the model was a theoretical zonal wind stress, which was independent of latitude. Hence they obtained only disturbances which were symmetric or antisymmetric about the equator. Three fundamental types of unstable disturbances were exhibited and compared with free modes in the absence of mean flow. Our results are necessarily different, since the symmetry is destroyed by the introduction of realistic mean currents. As previously

discussed by Brossier (1987), a tropical mean flow, not symmetric about the equator, strongly modifies the dispersion diagram of equatorial modes. Therefore, the 1 200 km-30 days eddy exhibited along 3°N in November cannot be identified with a theoretical free mode in the absence of mean flow.

Let us assume now that this eddy is a response to an external atmospheric forcing. In the November experiment, oscillations on a time-space scale of 30 days-1 200 km are present in the sea-level variability deduced from Geosat data ; we obtain the same time-space scale in the fluctuations of the currents computed by the model. This result is not inconsistent with the assumption of an external forcing. However, the oceanic response corresponding to the same Geosat sea-level variability, and consequently to the same external forcing, is quite different if the tropical mean circulation is modified: the eddy is either present but weakly energetic (in May), or no longer present ($U_0 = 0$). Moreover, if the forcing is external, and if we impose a theoretical sea-level variability with a random time-dependence and therefore no particular frequencies, there is no reason to find the 1 200 km-30 days eddy in the fluctuations of the currents. The results previously described for the November experiment show that this eddy is the main feature of the oceanic response, whatever the sea-level fluctuations. So, the assumption of an external atmospheric forcing must be rejected. The oceanic wave 1 200 km-30 days is generated by the mean tropical current system.

The sea-level oscillations, evidenced by altimetric measurements, are the trace of the oceanic eddies.

A number of studies, either using numerical models, or analysing *in situ* observations have already demonstrated a considerable interaction between the mean flow and the variability in tropical oceans. The barotropic instability produced by the latitudinal shear between the SEC and the NECC can generate instability waves of period 30 days, wavelength about 1 100 km (Philander, 1978). Together with barotropic instability, baroclinic instability is also a source of perturbation energy (Cox, 1980). Estimations of the eddy - mean flow energetics in the Pacific Ocean were given by Hansen and Paul (1984). They found both barotropic and baroclinic instability processes to be of equal importance. In the Atlantic Ocean, a wave of period 25 days, wavelength 1 000 to 1 200 km, was evidenced from current meter data (Weisberg and Weingartner, 1988). This wave was found to be maximum along the equator, and confined primarily to the upper mixed layer. The authors concluded that these eddies were generated by the barotropic instability within the cyclonic shear region of the SEC and that baroclinic instability was negligible.

We find, as in the observations, that the wave 1200 km-30 days is seasonally modulated. Highly energetic eddies are obtained in November, when the meridional shear of the mean zonal current is strong. The imposed Geosat sea

level anomalies are then in seasonal coherence with the mean flow, as they were deduced from October-February measurements. Maxima values of surface oscillations are located along 5°N-6°N, north of the oceanic wave which travels along 3°N. Analysis of the observations performed in the Pacific Ocean gives the same shifting in the location of the eddies : 3°N for the velocity oscillations, 5-6°N for the sea-level oscillations. The eddy energy computed by the model is trapped in the upper layer. Free waves are excited along the equator in the absence of mean flow. They are still present in May, but in November these modes are no longer present. Thus, we cannot obtain a radiation of eddy energy into the deep ocean via free planetary waves, as described by Cox (1980).

The only realistic simulation of the tropical Pacific Ocean we have carried out is that obtained with the mean circulation of November and the sea-level variability deduced from Geosat observations. Altimetric measurements were selected during autumn-winter (October 1987 to February 1988), in order to retain the strongest signal. The model is linearized around the mean circulation, and so eddies are filtered and weakened. A high level of forcing signal is necessary to obtain a clear answer. To be coherent, sea level fluctuations and mean currents have to be taken at the same season. In this simulation, the oceanic eddies corresponding to the time-space scale 30 days-1 200 km
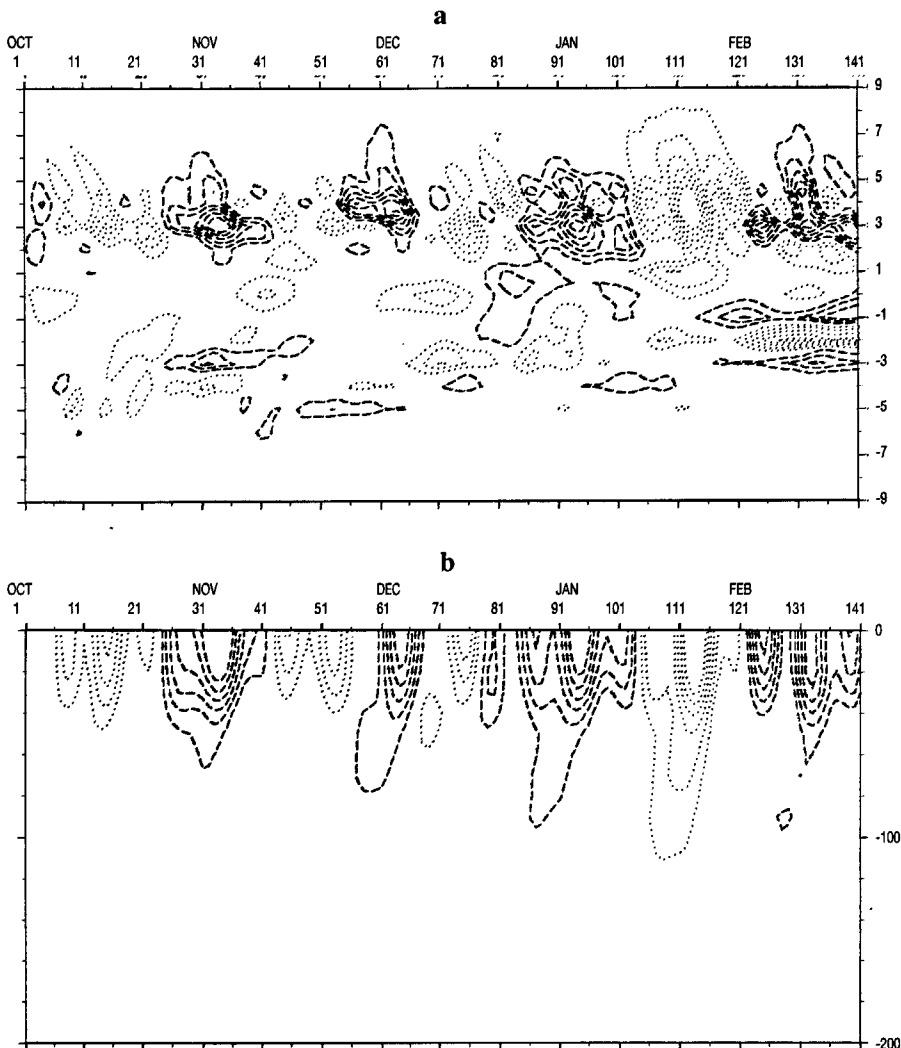

Figure 14.

Mean flow : November ; sea-level 3.

v at a fixed longitude (x=0). Dotted lines: v < 0 ; dashed lines: v > 0 ; the zero line is not plotted ; contour interval is 5 cm.s⁻¹.

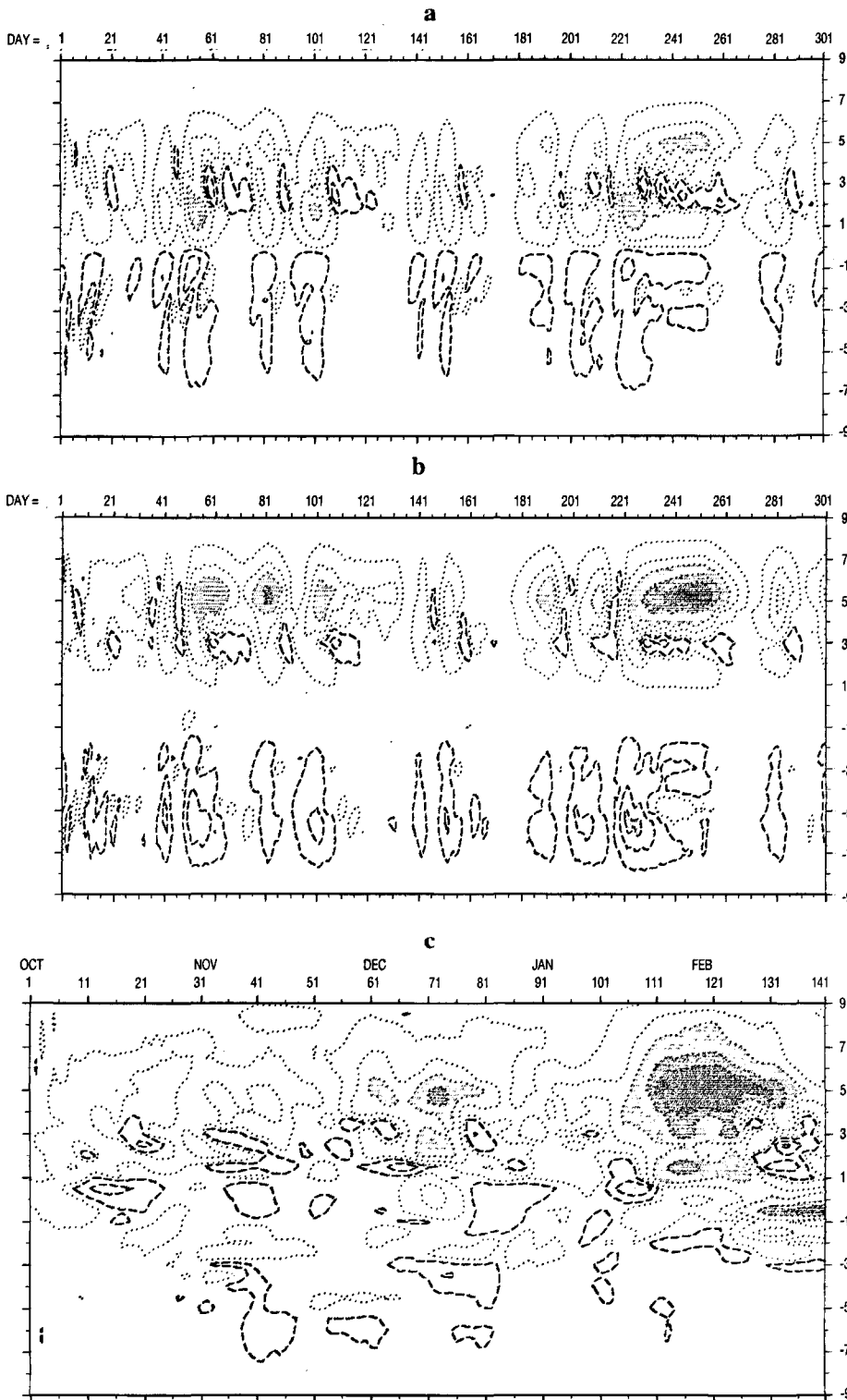*a - v as a function of latitude and time ; z = 5 m. b - v as a function of depth and time ; latitude : 3°N.*

Figure 15.

Mean flow : November.

Heat transport H as a function of latitude and time. Dotted lines: H southward ; dashed lines: H northward ; isocontours are -30, -20, -10, -5, -1, 1, 5, 10.10^{12} Watts ; shaded areas: $|H| > 10.10^{12}$ Watts.

a - sea-level 1 ; b - sea-level 2 ; c - sea-level 3.

are present along 3°N. They are highly energetic from 15 January to 15 February. The heat transport associated with the eddies is southward. This corresponds to the results described by Hansen and Paul (1984) for the Pacific Ocean, and by Weisberg and Weingartner (1988) for the Atlantic Ocean. The maximum of southward heat flux given by the model is of order 30.10^{12} Watts and is obtained between 3°N and 7°N, from 15 January to 15 February, when the eddies are the most active. A heat transport of 20.10^{12} Watts across the equator, from the northern to

the southern hemisphere, is observed somewhat later (February). In conclusion, the eddies seem to induce a redistribution of heat in the equatorial zone that is obviously seasonally modulated, as are the eddies themselves. The computed heat transport is induced only by the perturbation and has to be added to the mean heat flux. When integrated over several eddies, the value of the southward heat transport is consistent with the estimation given by Philander et al. (1986). Our estimation also corresponds to the value deduced from the diagrams publi-

shed by Dvoryaninov and Eremeev (1992). The south-ward heat transport exists only for a short period, slightly after strong wave activity during winter. Other periods of the year are less favourable to wave development and we may have captured the totality of the southward transport by the eddies in our simulation. Nevertheless our estimate may be too low, as a linearized model acts as a filter and the energy input from Geosat altimetric variances may contain some flaws.

Obviously, such a simplified model gives incomplete results on the variability of the tropical ocean. The model is linearized and cyclic in the zonal direction and the variability of the flow has to correspond to the imposed sea-level variability. We are developing a more sophisti-cated method, using optimal control theory. It will cer-tainly be interesting to compare the results, but the model described here is simple and cheap to carry out, while the other one requires long and complex computations. In spite of simplifying assumptions, the model makes it pos-sible to obtain the instability waves 1 200 km-30 days, to study their seasonal variations in relation with the charac-teristics of the mean flow, and to compute the southward heat flux induced by the eddies.

APPENDIX

Before applying the hydrostatic assumption, the equations satisfied by (V'= (u',v',w'),p'), perturbations of the mean current and pressure, are of Navier-Stokes type. The phy-sical problem (pb 1) is posed in an open set $\Omega_S = \omega_S \times$]0,L[, L being the zonal extension of the domain (Fig. 16). Boundary conditions are imposed : these conditions are periodic in the x-direction, of Neumann type on the other parts of the boundary. If we assume that the perturbation is forced by a perturbation of the wind, the boundary condi-tions on Γ_S , the free surface of the ocean, are given by V'. n = 0, V_n = f ' where n is the unit vector normal to Γ_S (n≠z), Vn the normal derivative, and f ' the perturbation of the wind-stress. We can prove the existence and unicity of the solution (V',p') of problem 1 (the equations are lineari-zed around the mean solution), but this problem 1 cannot be numerically solved without other assumptions since the perturbation of the wind and the free surface Γ_S are unk-nown (only the variability ξ' is given by altimetry).

We shall therefore construct another problem (pb 2), the numerical solution of which has to be an approximation of

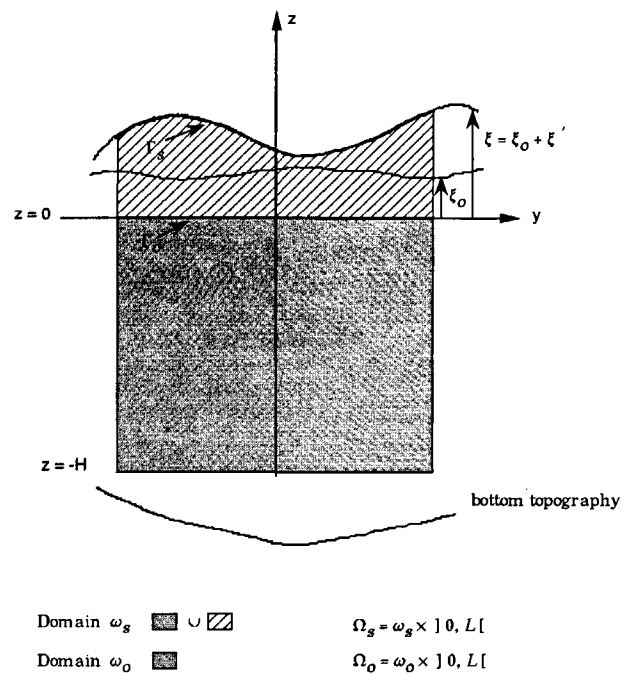

Figure 16

Domains Ω_S and Ω_0 (Appendix).

the solution (V',p') of problem 1. The physical domain Ω_S is replaced by Ω_0. The vertical extension of Ω_0 is : $- H \le z \le 0$. The free surface remains Γ_S but the perturbation is not computed in the upper layer $(O \le z \le \xi)$. As previous-ly, we can demonstrate the existence and unicity of the perturbation $(\tilde{V}, \tilde{p}')$, solution of problem 2 in Ω_0. Rela-tion (6) gives an approximation of the pressure gradient $\nabla p'$, deduced from the variability ξ' of the free surface. In problem 2, we impose that $\nabla \tilde{p}'$ is given by relation (6), so $\tilde{p}'$ approximates p'. To compute the velocity $\tilde{V}$, we have to impose boundary conditions on Γ_0. We have choosen : $\tilde{V}.n = 0$, $\tilde{V}_n = 0$ $(\tilde{V}_n$ normal derivative, n = z). Numeri-cally, these conditions are not too restrictive : they are applied not to the total current, but only to its variability ; the vertical step Δz used to calculate the vertical gradient is small in the upper layer.The perturbation $(\tilde{V}, \tilde{p}')$, solu-tion of problem 2, is an approximation of (V , p '), solution of problem 1. The numerical scheme used to solve pro-blem 2 is described in the paper. It uses the hydrostatic assumption and a cyclic expansion in the x-direction.

REFERENCES

Brossier F. (1986). Mathematical modelisation of equatorial waves. *Acta Appl. Math.,* **5,** 37-85.

Brossier F. (1987). Numerical modeling of equatorial waves in the presence of a mean current. *J. Phys. Oceanogr.,* **17,** 1100-1113.

Cox M.D. (1980). Generation and propagation of 30-Day waves in a numerical model of the Pacific. *J. Phys. Oceanogr.,* **10,** 1168-1186.

Dandin P. (1991). Modélisation de l'Océan Pacifique Tropical. Rap-port interne *LODYC,* Université Paris 6.

Dukowicz J.K. and R.D. Smith (1994). Implicit free-surface method for the Bryan-Cox-Semtner ocean model. *J. Geophys. Res.,* **99,** C4, 7991-8014.

Dvoryaninov G.S. and V.N. Eremeev (1992). Tropical instability waves and effects related to them. *TOGA* notes, **6,** 4-7.

Hansen D.V. and C.A. Paul (1984). Genesis and effects of long waves in the equatorial Pacific. *J. Geophys. Res.,* **39,** 10431-10440.

Harvey R.R. and W.C. Patzert (1976). Deep Current measu-rements suggest long waves in the eastern equatorial Pacific. *Science,* **193,** 883-884.

Legeckis R. (1977). Long waves in the eastern equatorial Pacific ocean : a view from a geostationary satellite. *Science*, **197**, 1179-1181.

Legeckis R., W. Pichel and G. Nesterczuk (1983). Equatorial long waves in geostationary satellite observations and in a multi-channel sea surface temperature analysis. *Bull. Amer. Met. Soc.*, **64**, 133-139.

Lighthill M.J. (1969). Dynamic response of the Indian ocean to the onset of the southwest monsoon. *Phil. Trans. Roy. Soc. London*, A, **265**, 45-93.

Lighthill M.J. (1978). *Waves in fluids*. Cambridge University Press, Cambridge, 504 p.

Malardé J.P., P. De Mey, C. Périgaud and J.F. Minster (1987). The oceanic dynamic topography associated with long equatorial waves. *J. Phys. Oceanogr.*, **17**, 2273-2279.

McCreary J.P., (1984). Equatorial Beams. *J. Mar. Res.*, **42**, 395-430.

McCreary J.P. and Z. Yu (1992). Equatorial Dynamics in a 2 1/2 - layer model. *Prog. Oceanogr.*, **29**, 61-132.

McPhaden M.J. and B.A. Taft (1988). Dynamics of seasonal and intraseasonal variability in the eastern equatorial Pacific. *J. Phys. Oceanogr.*, **18**, 1713-1732.

Miller L., D.R. Watts and M. Winbush (1985). Oscillations of dynamic topography in the eastern equatorial Pacific. *J. Phys. Oceanogr.*, **15**, 1759-1770.

Musman S. (1989). Sea height wave form in equatorial waves and its interpretation. *J. Geophys. Res.*, **94**, 3303-3309.

Pacanowski R.C. and S.G.H. Philander (1981). Parametrization of vertical mixing in numerical models of tropical oceans. *J. Phys. Oceanogr.*, **11**, 1443-1451.

Périgaud C. (1990). Sea-level oscillations observed with Geosat along the two shear fronts of the Pacific North Equatorial countercurrent. *J. Geophys. Res.*, **95**, 7239-7248.

Philander S.G.H. (1976). Instabilities of zonal currents, 1. *J. Geophys. Res.*, **81**, 3725-3735.

Philander S.G.H. (1978). Instabilities of zonal currents, 2. *J. Geophys. Res.*, **83**, 3679-3682.

Philander S.G.H. and R.C. Pacanowski (1980). The generation of equatorial currents. *J. Geophys. Res.*, **85**, 1123-1136.

Philander S.G.H. and R.C. Pacanowski (1986). The mass and heat budget in a model of the Tropical Atlantic Ocean. *J. Geophys. Res.* **91**, 14 212-14 220.

Philander S.G.H., W.J. Hurlin and R.C. Pacanowski (1986). Properties of long equatorial waves in models of the seasonal cycle in the tropical Atlantic and Pacific oceans. *J. Geophys. Res.*, **91**, 14 207- 14 211.

Philander S.G.H., W.J. Hurlin and A.D. Siegal (1987). Simulation of the Seasonal Cycle of the Tropical Pacific Ocean. *J. Phys. Oceanogr.*, **17**, 1986-2002.

Philander S.G.H. and W.J. Hurlin (1988). The heat budget of the Tropical Pacific Ocean in a Simulation of the 1982-83 El Nino. *J. Phys. Oceanogr.*, **18**, 926-931.

Siegal A.D. (1985). A comment on long waves in the Pacific Ocean. *J. Phys. Oceanogr.*, **15**, 1881-1883.

Weisberg R.H. (1986). Observations pertinent to instability waves in the equatorial oceans in: *A report of the U.S. Toga Workshop on the Dynamics of the Equatorial Oceans*, E.J. Katz and J.M. Witte Editors, Honolulu, Hawaï, 335-350.

Weisberg R.H. and Weingartner T.J. (1988). Instability waves in the Equatorial Atlantic Ocean. *J. Phys. Oceanogr.*,18, 1641-1657

Wyrtki K. (1978). Lateral oscillations of the Pacific Equatorial Countercurrent. *J. Phys. Oceanogr.*, **8**, 530-532.